This is a Preprint and has not been peer reviewed.

Title

Relative role of rock erodibility and sediment load in setting channel slope of mountain rivers

Author

Naoya O. Takahashi
Department of Earth science, Graduate school of Science, Tohoku University
naoya.takahashi.c5@tohoku.ac.jp

Abstract

Rock strength influences channel slope by altering substrate erodibility and the size of sediments supplied to the channels. Although the frequent presence of knickpoints at lithological boundaries indicates that rock erodibility significantly determines channel morphology, a growing body of field evidence suggests that the coarse sediment supply from less erodible rock units is a primary factor in channel steepening. To assess the relative effects of rock erodibility and imposed sediment load on channel slope, I studied five rivers in Tsugaru, northern Japan. These rivers flow through alternating volcanic rock and sedimentary rock. The minimum channel slope required to transport both *in situ* sediments and those supplied from upstream was calculated using slope component analysis. The findings suggest that sediment effects largely account for the observed variations in channel slope across both volcanic and sedimentary rocks. The proportion of channel slope not explained by the imposed sediment load was slightly higher in volcanic rock reaches than in sedimentary rock reaches, which can be attributed to the lower erodibility of volcanic rock. Based on the grain size distributions of volcanic and sedimentary rock particles and the calculated impacts of sediment load, I conclude that the coarse sediment supply from volcanic rock is the primary cause of the difference in channel steepness between the rock types in Tsugaru. Although this conclusion holds generally

true across Tsugaru, certain reaches with locally high channel steepness exhibit more extensive bedrock exposure than adjacent gentler reaches, suggesting that contrasts in erodibility also play a significant role in determining the channel slope. Therefore, examining what factors alter the relative significance of rock erodibility and sediment load can enhance our understanding of how rock properties influence longitudinal stream profiles.

Keywords: *Rock type, erodibility, sediment load, grain size, bedrock river*

1 INTRODUCTION

Bedrock properties significantly control topography and the rate of landscape change. In erosional landscapes, the morphology of channels and erosion rates are associated with rock erodibility, which depends on rock properties such as the degree of fracturing and tensile strength (Molnar et al., 2007; Sklar & Dietrich, 2001; DiBiase et al., 2018a; Turowski et al., 2023). Longitudinal stream profiles are typically steeper in rocks with low erodibility, allowing erosion to occur at rates comparable to those in rocks with higher erodibility or to align with the rate of baselevel changes (Hack, 1973; Howard & Kerby, 1983; Duvall et al., 2004; Bursztyn et al., 2015; Harel et al., 2016; Yanites et al., 2017; Gallen, 2018). Although rock erodibility is crucial in the evolution of fluvial landscapes, it does not always manifest in stream profiles. This discrepancy is partly because other factors such as climate, tectonics, and sediment dynamics might offset the effects of differential erodibility or exert a more dominant influence on channel slopes (Whipple & Tucker, 2002; Kirby et al., 2003; Sklar & Dietrich, 2006; Takahashi et al., 2022; Leonard et al., 2023). Moreover, landscape evolution models have demonstrated that the apparent disconnect between rock erodibility and channel slope or erosion rates can result only from the contrast in erodibility when rivers carve through rocks with varying erodibilities (Forte et al., 2016; Perne et al., 2017; Fox et al., 2023; Smith et al., 2024). Thus, understanding how and to what extent rock erodibility determines channel slope is essential for identifying the drivers of landscape evolution.

Rock erodibility indirectly influences the channel slopes by affecting the size of sediment produced on hillslopes. When bedrock rivers transport a large volume of sediment, they typically become steeper to expose and incise the bedrock (Hack, 1957; Sklar & Dietrich, 2006; Shobe et al., 2021a; Carr et al., 2023; Sklar, 2024). To assess the impact of sediment load on channel slope, Sklar and Dietrich (2006) calculated the minimum channel slope required to entrain bed materials and transport sediment from upstream to downstream. They explored how the proportion of the channel slope attributable to the imposed sediment load varied with the rock tensile strength based on the saltation–abrasion river incision model. Their model predicted that channel slope remained relatively unchanged with variations in rock tensile strength, with sediment load playing a dominant role in influencing channel slope (Sklar and Dietrich, 2006). Subsequent studies incorporating sediment terms into river incision models have confirmed a less pronounced impact of rock erodibility on channel slope compared to predictions from models that disregard the sediment effects (Turowski et al., 2007; Guryan et al., 2024). Less erodible rocks tend to produce larger, denser, and more durable grains than erodible rocks (e.g., Attal & Lavé, 2009; Sklar et al., 2017). These characteristics of less erodible rocks lead to a longer residence time in channels and a potentially greater impact on channel slope, which is supported by numerous studies (e.g., Duvall et al., 2004; Johnson et al., 2009; Thaler & Covington, 2016; Finnegan et al., 2017; Shobe et al., 2021a; Lai et al., 2021; Anderson et al., 2023). Thaler and Covington (2016) observed that the normalized channel steepness increased with both boulder size and the areal fraction of boulder coverage in rivers cutting through bedrock of varying mechanical strengths. Lai et al. (2021) reported that the channels in sedimentary rocks became steeper when receiving coarse sediments from upstream volcanic rock units that are mechanically stronger and less erodible than sedimentary rocks. Baynes et al. (2020) showed rivers draining relatively hard graywacke units have wider channel width than those do not. These observations suggest that the influence of coarse sediment from upstream less erodible rock units persists even after transitioning to erodible bedrock, affecting the disparity in channel geometries between rock types.

This study assessed the relative impacts of rock erodibility and imposed sediment load on channel morphology to reveal how rock type influences river morphodynamics. Following the methodologies of Sklar and Dietrich (2006) and Lai et al. (2021), I calculated the minimum channel slope required to transport the imposed sediment load, using hydraulic geometry and grain size data from five rivers draining areas with less erodible volcanic rock and erodible sedimentary rock units in Northern Japan. The findings indicated that sediment effects could account for most of the variation in channel slope across both rock types. Additionally, the proportion of the slope component not explained by sediment load was larger in reaches of volcanic rock compared to those of sedimentary rock, which was attributed to differences in rock erodibility. The discussion then explores how rock erodibility and sediment load govern the slopes of mountain rivers.

2 Geologic setting

Tsugaru Mountain is located in northern Japan and primarily comprises Neogene sedimentary and volcanic rocks, including shale, mudstone, and sandstone (Figure 1). Around Hakamakoshi-dake, which has the peak with an elevation of approximately 630 m, basalt and dolerite have intruded into the Miocene sedimentary rocks, creating a dome structure near the headwaters (Tsushima & Uemura, 1959; Uemura et al., 1959; Fujii, 1981; Nemoto, 2014). The intruded volcanic rock also forms sills of varying thicknesses parallel to the bedding of the sedimentary rock (Tsushima & Uemura, 1959; Uemura et al., 1959). The basaltic rocks display various forms; some are massive and joint-free, whereas others are densely jointed or deeply weathered (Figure 2). The Tsugaru Fault is a west-dipping reverse fault trending north-south that is situated on the eastern flank of Hakamakoshi-dake, separating the basaltic dome to the west from the Plio-Pleistocene sedimentary rocks to the east (Uemura et al., 1959; Nemoto, 2014). Active since the late Pliocene, this fault has continued its activity up to the deposition of the Tsurugasaka formation at 0.76 Ma (Suzuki et al., 2005; Mimura, 1979; Nemoto, 2014). With a vertical displacement exceeding 1000 m, the fault has caused the adjacent sedimentary and volcanic layers to tilt westward (Mimura, 1979; Ujiie et al., 2006). Currently, the deformation front is located at the eastern base of the mountain range (Headquarters for Earthquake Research Promotion, 2004).

This study examines five rivers on the western flank of Tsugaru Mountain (Figure 1). The studied river sections were chosen to avoid tuff units and influence of check dams. The river courses, specifically Mosawa, Shikibasawa, Yunosawa, and Ohkurasawa, alternate between volcanic and sedimentary rocks. The channel slopes of these rivers are generally steeper over volcanic substrates than sedimentary ones (Figure 3; Supporting Information Figure S1). However, in certain sections such as in Yunosawa, channel slope does not correlate well with substrate rock type, indicating that substrate erodibility may not solely determine longitudinal stream profiles.

In Tanosawa, another surveyed river, the presence of sedimentary rock is minimal. Both the main stream and a tributary of Tanosawa traverse similar basaltic rocks, yet the main stream, Tn1, is steeper than the tributary, Tn2 (Figure 3a), suggesting that factors other than rock erodibility influence the variations of channel slope. Understanding why Tn1 is steeper than Tn2 could reveal the factors influencing channel slope dependency on rock type. Therefore, I included Tanosawa in this study. It was hypothesized that spatial heterogeneity in rock fracturing caused the variation in bed material size, resulting in the observed slope differences (Figure 2). To test this hypothesis and quantify the impact of the sediment on the channel slope, the same survey methodology was applied in Tanosawa as in the other four rivers.

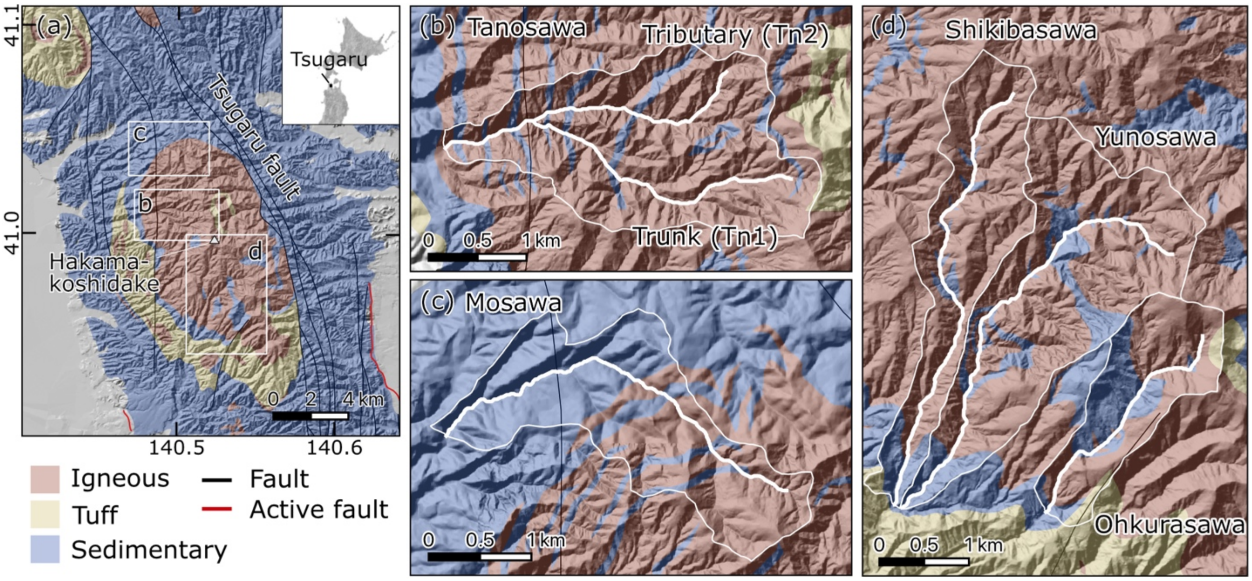

Figure 1. Geology of the study area. Faults and active faults are after Geological survey of Japan (2023) and Nakata and Imaizumi (2002), respectively. (a) Geologic map is modified after a 1:200,000 map (Geological survey of Japan, 2023). Inset shows the location of the Tsugaru Mountain. (b–d) River sections and their catchment areas investigated in this study. Geologic map is modified after 1:50,000 maps (Tsushima & Uemura, 1959; Uemura et al., 1959; Fujii, 1981).

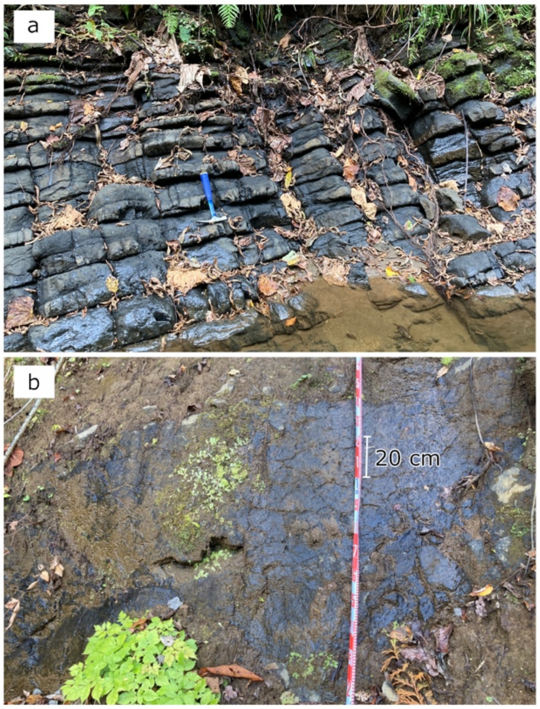

Figure 2. Bedrock outcrops of basalt in Shikibasawa. (a) Densely jointed bedrock exposed in a stream channel. Length of hammer: ~30 cm. (b) Bedrock outcrop with minor surficial cracks.

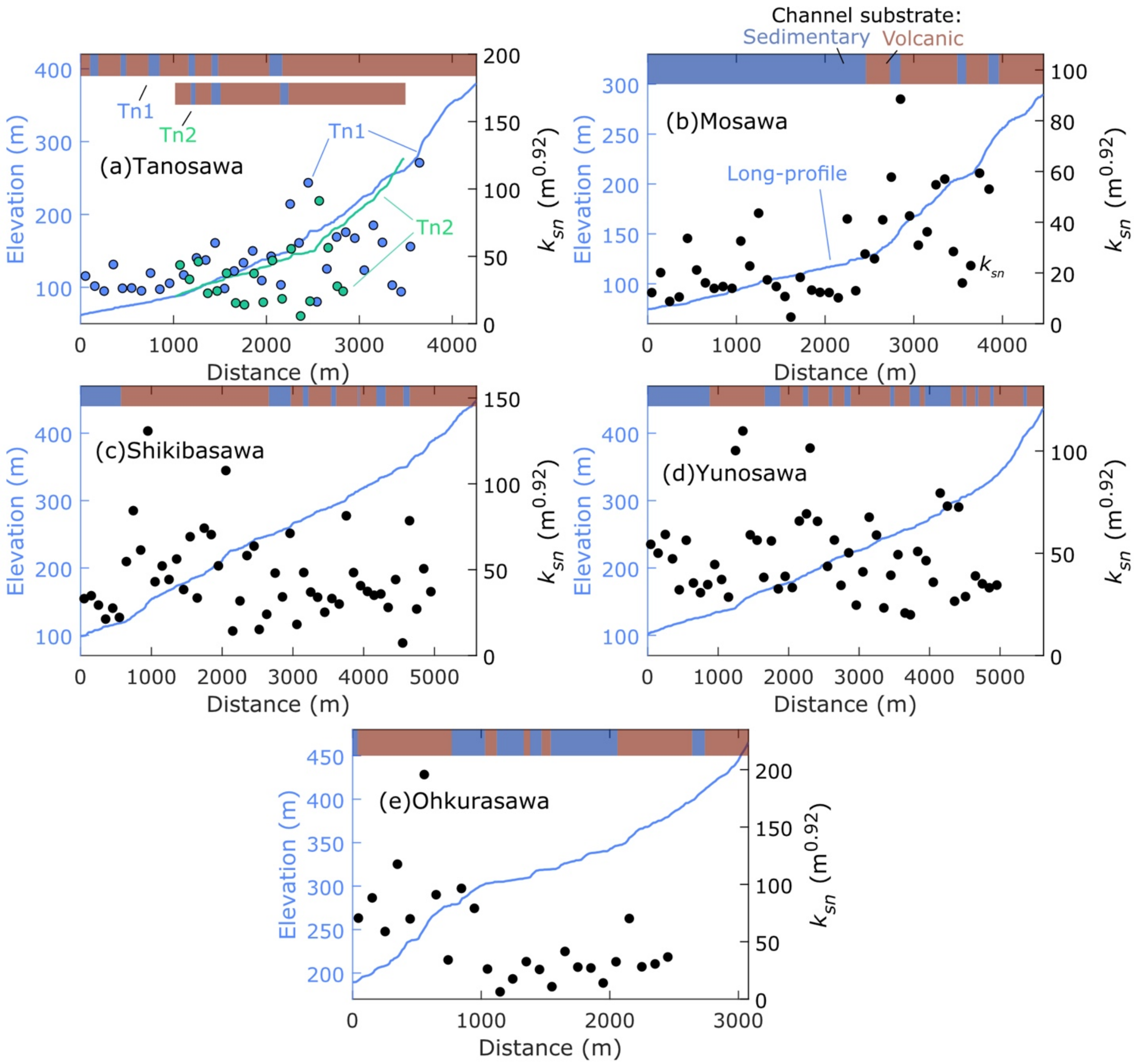

Figure 3. Longitudinal profiles (lines) and normalized channel steepness (circles) along the studied sections. Bar at the top represents channel substrate. (a) Blue and green circles represent normalized channel steepness of the trunk stream (Tn1) and the tributary (Tn2). Blue and green lines are stream profiles of Tn1 and Tn2.

3 Method

To investigate the influence of rock erodibility on channel slope, I calculated normalized channel steepness (k_{sn}), hillslope angles along the stream, and wideness of channels (k_w). Additionally, a slope component analysis was conducted, which segmented the current channel slope into two components associated with the imposed sediment load and a third residual component not explained by sediment load (Sklar and Dietrich, 2006). It was hypothesized that the proportion of the residual slope component would increase as the rock erodibility decreased. This hypothesis was tested by comparing the proportions of the residual slope component between reaches composed of volcanic and sedimentary rocks.

3.1 Topographic analysis

I calculated the normalized channel steepness using the Topotoolbox (Schwanghart and Scherler, 2014),

$$z(x) = z(x_0) + k_{sn}\chi \tag{1}$$

$$\chi = \int_{x_0}^{x} (A_0/A(x))^{\theta ref}\, dx \tag{2}$$

where $z(x)$ and $A(x)$ is elevation and upstream drainage area at the distance x from the most downstream point x_0 ($x_0 = 0$), respectively. A_0 is reference drainage area which was set to 1 m^2 in this study. χ is a horizontal coordinate of a longitudinal river profile (Perron and Royden, 2013). The exponent θ_{ref} is a reference concavity index (Snyder et al., 2000). I used a 10-m-meshed digital elevation model (DEM) provided by the Geospatial Information Authority in Japan. The DEM is created using elevation contours of topographic maps. The accuracy of elevation (root mean square error) is less than 5 m. The river reaches were segmented every 100 m along the streams. For each channel segment, I calculated k_{sn} by a linear regression in a χ-elevation space (a chi plot, Perron and Royden, 2013). A reference concavity of 0.46 was used, as determined by averaging the optimum concavity index for each stream that best linearizes the river profile in a chi plot. The analysis focused on river sections with a drainage area greater than 0.4 km^2, excluding colluvial reaches (Supporting Information Figure S1f; Stock and Dietrich, 2003). A one-sided Wilcoxon rank-sum test was conducted for each river to evaluate if k_{sn} values are larger in volcanic rock reaches than in sedimentary rock reaches at a 5% significance level. The null hypothesis posited that volcanic rock reaches have the same median k_{sn} values as sedimentary rock reaches. The alternative hypothesis was the median k_{sn} is higher in volcanic rock reaches. To examine the effect of channel segment on the results, I performed the same calculation using the different length of a channel segment (150, 200, and 300 m).

The variations in hillslope angles along the trunk streams were analyzed to assess their impact on channel steepness, as these angles influence the rates and processes of hillslope sediment supply (Roering et al., 2001; Montgomery & Brandon, 2002). The hillslopes connected directly to the trunk stream were initially mapped based on slope aspect derived from the 10-m-meshed DEM. These hillslopes were then subdivided every 200 m along the streams, and the 16th, 50th, and 84th percentile values of hillslope angles were calculated.

High-flow width W was measured using a TruPulse®200 laser range finder (Laser Technology, Inc). Measurement error of the instrument is 30 cm. When measuring channel width, I focused on a section 50–100 meters along the channel and looked for a site where its channel width is close to the average width of the section. I selected a site where the channel was relatively straight, single-threaded, and free of recent bank failure and obstacles that affects local hydraulic conditions such as colluvium, log jams, and exceptionally large boulder relative to the average bed material. At the selected site, the maximum and minimum estimates of water level at a high-flow stage were determined based on heights of flood debris, washed out tree roots, vegetation limits, and channel bank. The widths at the maximum and minimum estimates of water level were recorded. The mean value of these widths was used in the subsequent analysis. For each river, the following equation was fitted to the mesured widths to estimate a scaling exponent b

$$W = k_w A^b \tag{3}$$

The coefficient k_w estimated in this regression was not used. Instead, the estimated b value was used to calculate local channel wideness k_w at each measurement site. Thus, the unit of k_w (m^{1-2b}) differs from river to river. Local k_w values were used to evaluate if channel width differs between rock types and affects channel steepness.

3.2 Slope component analysis

To assess the impact of sediment load on longitudinal channel profiles, I conducted a slope component analysis following the methodologies of Sklar & Dietrich (2006) and Lai et al. (2021). For bedrock incision to occur, the channel slope must be sufficiently steep to transport both the sediments at the riverbed and those transported from upstream reaches and expose bedrock. Based on this premise, Sklar and Dietrich (2006) decomposed the steady-state channel slope (S) into three components:

$$S = S_{D_s} + \Delta S_{Q_S} + \Delta S_E, \tag{4}$$

In this study, S is local channel slope within 50 meters from the sites where slope components are calculated. When the selected river section includes a tributary confluence, the section was truncated at the confluence. Local slope was calculated by a linear regression of elevation against flow distance. S_{D_s} denotes the threshold slopes for the incipient motion of the bed materials. ΔS_{Q_S} indicates the additional slope above S_{D_s}

to transport sediment supplied from upstream. ΔS_E indicates the residual slope. S_{D_s} denotes the slope that makes the Shields number for a sediment particle (τ^*) equal to the critical Shields number (τ_c^*).

$$\tau^* = \frac{SR}{R_b D_s} \quad (5)$$

$$S_{D_s} = \frac{\tau_c^* R_b D_s}{R} \quad (6)$$

D_s is the representative grain size. Specifically, I used the 84th percentile grain size (D_{84}) because coarser grains in a given grain size distribution posed a greater influence on the channel morphology (MacKenzie et al., 2018; Shobe et al., 2021b). R_b denotes the relative buoyancy density of the sediment.

$$R_b = \frac{\rho_s - \rho_w}{\rho_w}, \quad (7)$$

where ρ_s and ρ_w represent the densities of the sediment and water, respectively. R denotes the hydraulic radius, assuming a rectangular channel cross section.

$$R = \frac{WH}{W + 2H}, \quad (8)$$

where H denotes the flow depth during the high-flow stage. To obtain H, the thalweg flow depth at the time of the survey was measured by a staff and added to the high-flow water level relative to the water level at the time of the survey. I used the mean value of the maximum and minimum depth. The width and depth near both the downstream and upstream ends of the river sections where grain size was measured were documented. The critical Shields number proposed by Lamb et al. (2008) was used.

$$\tau_c^* = 0.15 S^{\frac{1}{4}} \quad (9)$$

ΔS_{Q_s} is computed using an equation for bedload sediment transport (Fernandez-Luque & van Beek, 1976; Sklar & Dietrich, 2006):

$$\Delta S_{Q_S} = (\tau^* - \tau_c^*)\frac{R_b D_s}{R}\left(\frac{Q_s}{Q_c}\right)^{\frac{2}{3}} \tag{10}$$

$\frac{Q_s}{Q_c}$ represents the ratio of sediment supply to transport capacity (hereinafter, relative sediment supply). The relative sediment supply could not be measured in the field; thus, the ratio of exposed bedrock (F_e) in the channel bed was used as a proxy (Chatanantavet and Parker, 2008).

$$\frac{Q_s}{Q_c} = 1 - F_e \tag{11}$$

F_e was recorded in the field as explained later. Subtracting the sum of S_{D_s} and ΔS_{Q_S} from the total slope yields ΔS_E (Equation 4). At some sites, the values of S_{D_s} exceeded total slope, resulting in the negative ΔS_{Q_S} values. Since subtracting negative ΔS_{Q_S} values from total slope may overestimate the residual component ΔS_E, the negative ΔS_{Q_S} values were turned to 0, and ΔS_E values were recalculated. Each slope component was multiplied by upstream catchment area to the power of θ_{ref} to obtain the three components of k_{sn} associated with S_{D_s}, ΔS_{Q_S}, and ΔS_E (Lai et al., 2021):

$$k_{sn} = \left(S_{D_s} + \Delta S_{Q_S} + \Delta S_E\right)A^{\theta_{ref}} = k_{sn}^{D_s} + k_{sn}^{Q_S} + k_{sn}^{E} \tag{12}$$

The same analysis was performed using the different length of channel segment (150, 200, and 300 m).

Wolman counting was employed at 44 sites to determine the grain size distributions. Intermediate axes of a minimum of 100 grains were measured from the surfaces of the gravel bars. To mitigate biases from inter- and intra-bar variability in grain size, gravel was sampled from multiple bars. The results represent the grain sizes of a river section extending at least 50 m along the stream. Additionally, the rock type of each grain was recorded at 32 sites to assess differences in grain size among rock types. Although several types of sedimentary and volcanic rocks were present, only two categories were used for simplicity: sedimentary and volcanic.

In the laboratory, the densities of these rock types were measured. In total, 51 grains of each type were collected, which exhibited densities of 1.82×10^3 kg/m^3 for sedimentary rocks and 2.28×10^3 kg/m^3 for volcanic rocks. Results of Wolman counting indicated that the proportions of volcanic rock grains at each site ranged between 56 and 98% and are 77% on average. Consequently, a weighted average density (ρ_s) of 2.17×10^3 kg/m^3 was calculated based on the average abundance of each rock type at each site.

The degree of bedrock exposure on the riverbed (F_e) was documented either visually or using an orthomosaic image, the latter being employed when the river channel was not obscured by vegetation. Owing to the narrow, vegetation-enclosed channels, using an unpiloted aerial vehicle was impractical. Instead, photographs were taken with a camera attached to a long pole, and the exposed bedrock areas were recorded on an iPad mini (6th generation, Apple Inc.). These images were then used to create an orthomosaic with AgiSoft Metashape software. The orthomosaic was imported into QGIS for F_e calculation. For visual estimates, an uncertainty of ±0.1 was noted. In cases where no exposed bedrock was visible, I assumed F_e was between 0 and 0.1, and used a value of 0.05 because of the difficulty of thoroughly inspecting the riverbed.

4 RESULTS

4.1 Channel steepness in a catchment of single rock type

The median k_{sn} values in the two Tanosawa channels (Tn1 and Tn2) were 39.2 m$^{0.92}$ and 20.3 m$^{0.92}$, respectively. (Figure 3, Table 1). The median k_{sn} was higher in Tn1 than in Tn2 regardless of the length of channel segment used to calculate k_{sn} (Table

S1). The average k_{sn} components related to sediment caliber, $k_{sn}^{D_s}$ and k_{sn}^{Qs}, were greater in Tn1 than in Tn2 by 4.0 and 9.2 $m^{0.92}$, respectively. In both streams, the sum of $k_{sn}^{D_s}$ and k_{sn}^{Qs} accounted for at least 86% of the total k_{sn} (Figure 4), indicating that the difference in k_{sn} between the two streams mostly resulted from differences in $k_{sn}^{D_s}$ and k_{sn}^{Qs}.

Furthermore, I focused on the variables that caused the difference in $k_{sn}^{D_s}$ and k_{sn}^{Qs} between Tn1 and Tn2. The median values for the three key parameters (R, D_{84}, and F_e) are listed in Table 1, which was used to evaluate S_{D_s} and ΔS_{Q_s} (Equations 6 and 10). The hydraulic radius R was 1.2 times greater in Tn1 than in Tn2, which reduced $k_{sn}^{D_s}$ and k_{sn}^{Qs} in Tn1 relative to those in Tn2. Wolman count was conducted at four and three sites in Tn1 and Tn2, respectively. The resulting D_{84} was 1.4 times greater in Tn1 than in Tn2. Given the uncertainty involved in estimating F_e, F_e is almost similar or slightly smaller for Tn1. As Q_c increases with the local channel slope, the similar bedrock exposure in Tn1 and Tn2, despite the greater channel slope in Tn1, suggests that Tn1 was more strongly affected by the sediment load supplied upstream.

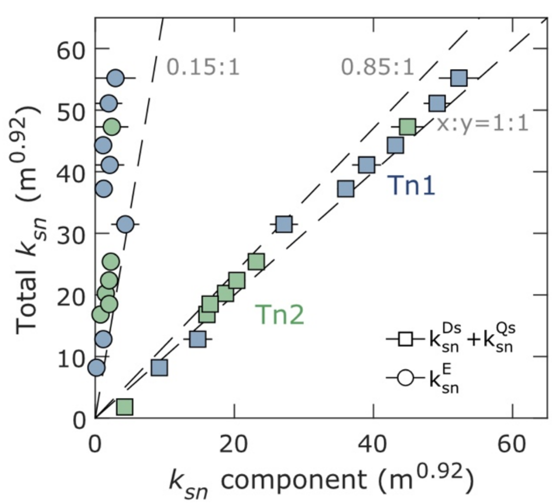

Figure 4. Comparison of k_{sn} components and total k_{sn} in Tanosawa.

Table. 1. Channel and sediment characteristics in Tanosawa. The numbers except for D_{84} are median values of the studied section.

	k_{sn} ($m^{0.92}$)	$k_{sn}^{D_s}$ ($m^{0.92}$)	k_{sn}^{Qs} ($m^{0.92}$)	R (m)	D_{84} (cm)	F_e (%)
Tn1	39.2	12.2	21.3	0.7	19	10
Tn2	20.3	8.1	12.1	0.6	14	20

4.2 Difference in k_{sn} components between rock type

In Mosawa, the median k_{sn} was 2.4 times as high in volcanic rock reaches compared to sedimentary rock reaches (Figure 3b, Supporting Information Table S1). The p value in a one-sided Wilcoxon rank-sum test was 1.0×10^{-3}, indicating the median k_{sn} was probably higher in volcanic rock. The residual k_{sn} component that is not explained by the imposed sediment load (k_{sn}^{E}) accounted for a small fraction of total k_{sn}, ranging from 1–16% in sedimentary rock reaches and 1–28% in volcanic rock reaches (Figures 5a and 6a, Supporting Information Table S2). These findings suggest that variations in k_{sn} were primarily caused by sediment effects.

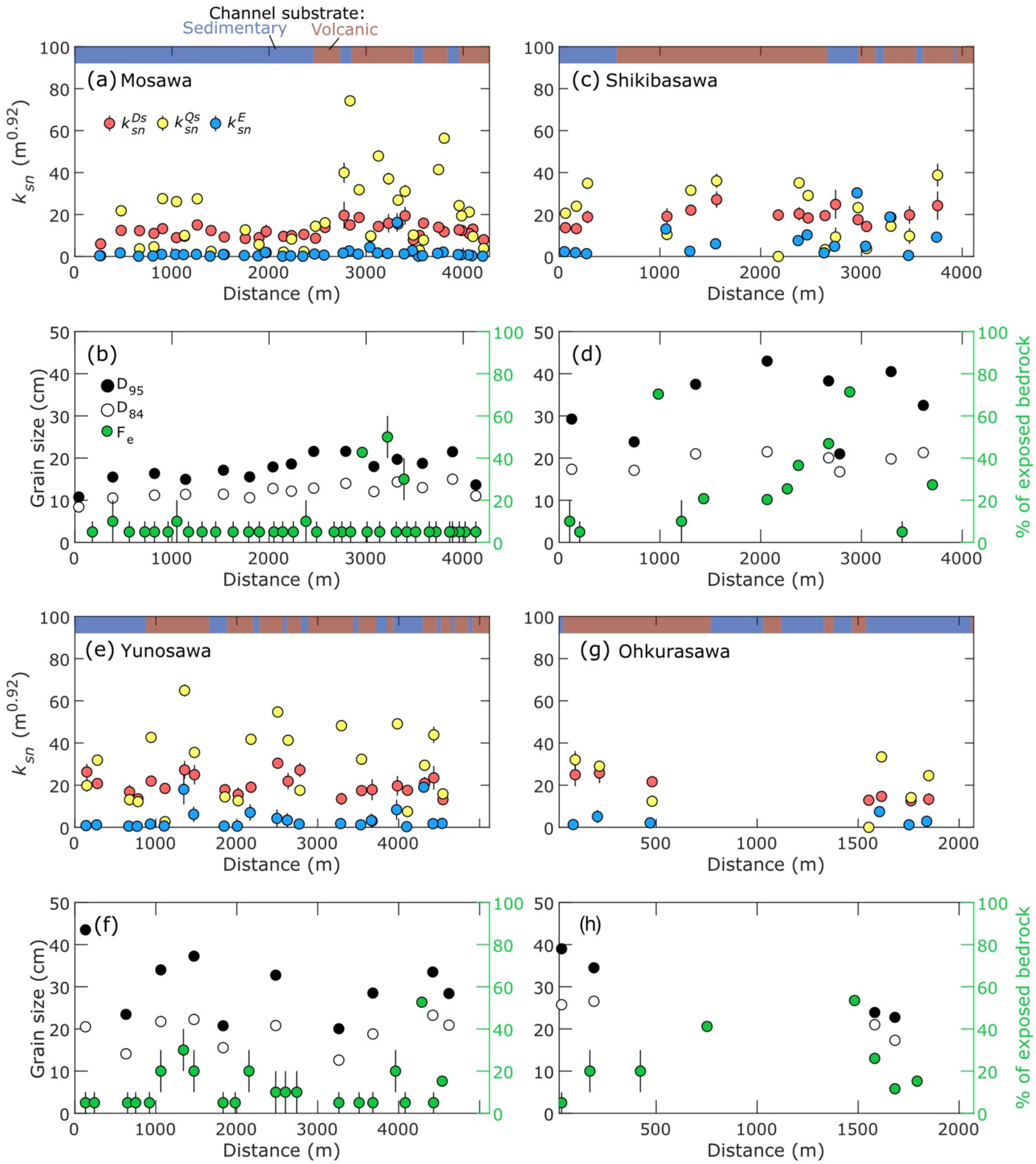

Figure 5. Variation of each k_{sn} component and key factors associated with the imposed sediment load. The top bar in (a), (c), (e), and (g) represents channel substrate.

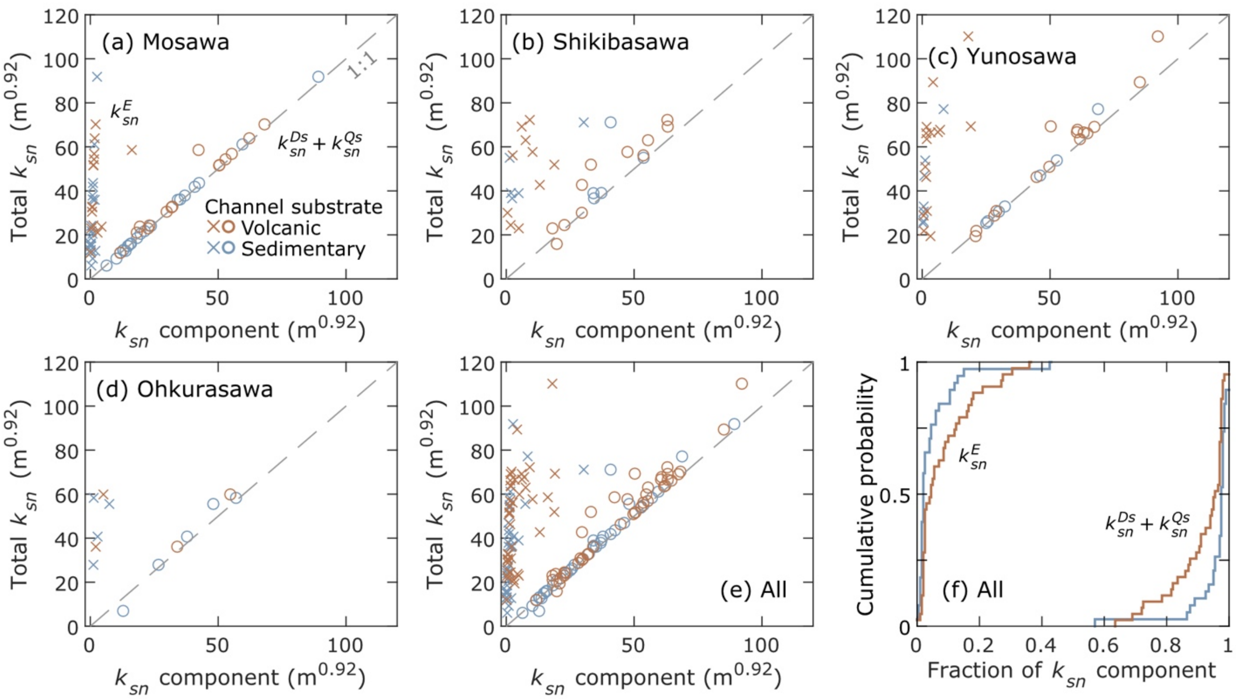

Figure 6. Comparison of k_{sn} components and total k_{sn} for volcanic and sedimentary rock. Results of (a-d) the individual rivers and (e) the four rivers. (f) Cumulative distribution function of the fraction of k_{sn} components.

In Mosawa, grain size did not significantly change in the most upstream section but began to decrease downstream near the lithologic boundary at 2460 m (Figure 5b). The hillslope angles were considerably steeper in the upstream section underlain by basaltic rock compared to the downstream section dominated by shale (Figure 7a).

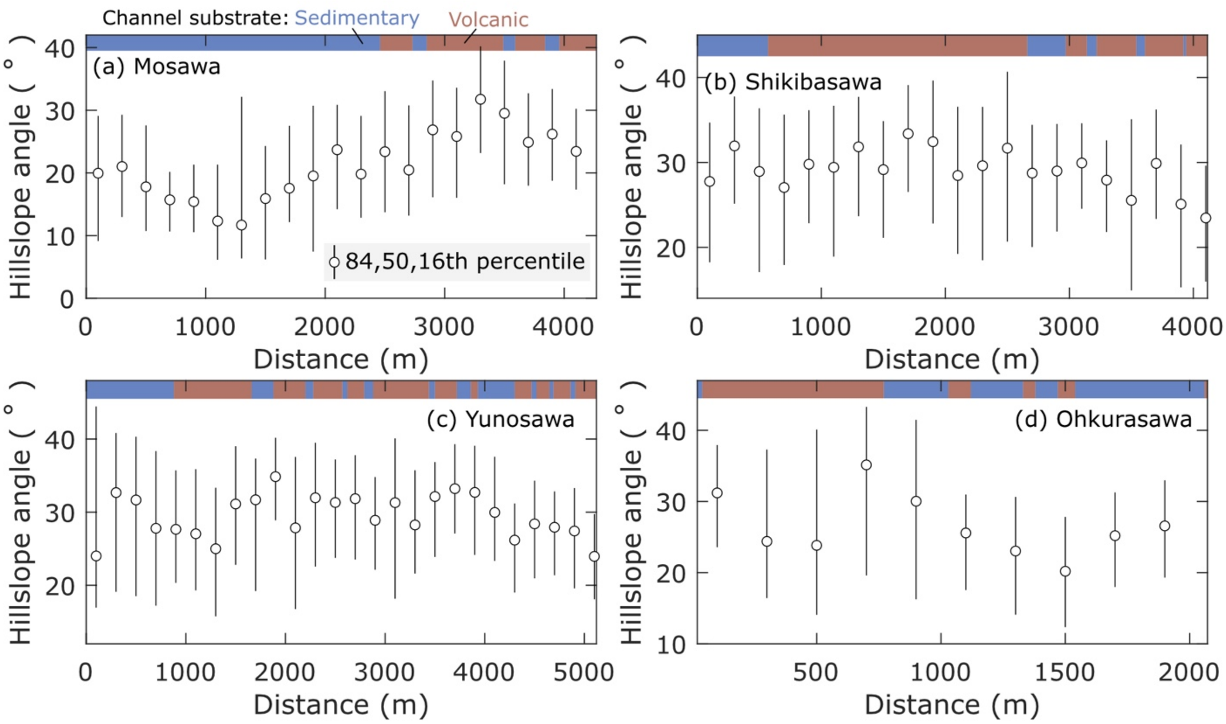

Figure 7. Angles of hillslopes along the trunk stream in each river catchment. The top bar represents channel substrate.

In Shikibasawa, the median k_{sn} in volcanic rock reaches was 1.3 times larger than that in the sedimentary rock reaches (Figure 3c). The p value in a one-sided Wilcoxon rank-sum test was 0.050. In the most upstream section, where sedimentary rock layers occurred intermittently, k_{sn} values did not exhibit clear variation with the rock type (Figure 3c). However, downstream from 2660 m, the k_{sn} values increased and then decreased at 600 m, coinciding with a transition from volcanic to sedimentary rock (Figure 3c). The residual k_{sn} (k_{sn}^{E}) accounted for 6.3% (median) of the total k_{sn} in sedimentary rock reaches and 12% in volcanic rock reaches (Figures 5c, 6b). Although the D_{84} did not systematically decrease across the studied sections in Shikibasawa, the 95th percentile grain size (D_{95}) downstream from 570 m was significantly smaller than upstream values. This reduction in D_{95} corresponded with the bedrock transition from volcanic to sedimentary rocks. Regarding bedrock exposure (F_e), despite significant local variations rendering it difficult to discern a general trend, bedrock was more extensively exposed in the upstream reaches (distance > 600 m) dominated by volcanic rock than in the most downstream reaches underlain by sedimentary rock. The hillslope angles increased slightly downstream in the headwaters (distance > 3000 m) and remained relatively constant throughout the studied section (Figure 7b).

In Yunosawa, the local variation in k_{sn} was large and did not correspond to the changes in the bedrock (Figure 3d). The ratio of k_{sn} in volcanic to sedimentary rock reaches change with the length of channel segment used to calculate k_{sn}. However, the p value in a one-sided Wilcoxon rank-sum test was 0.47–0.87 (Supporting Information TableS1), indicating k_{sn} values were indistinguishable between rock types. The median ratio of k_{sn}^E to total k_{sn} was 1.9% in the reaches of sedimentary rock and 4.8% in the reaches of volcanic rock (Figures. 5e, 6c).

The grain size in Yunosawa varied widely over short distances and did not follow a systematic trend as predicted by Sternberg's law (Figure 5f). The hillslope angles were consistent across the studied sections (Figure 7c). Although observations of F_e were limited, the bedrock was relatively well-exposed in an area between approximately 1000–1500 m, which roughly corresponded to the section with a higher k_{sn} (1250–1500 m in distance) compared to neighboring sections (Figures 3d and 5f).

In Ohkurasawa, k_{sn} increased downstream at 800–1000 m, where the channel substrate changed from sedimentary to volcanic (Figure 3e). The median k_{sn} was 27.5 and 58.9 $m^{0.92}$ for the sedimentary and volcanic rock, respectively. The p value in a one-sided Wilcoxon rank-sum test was 0.024, indicating the median k_{sn} values were probably higher in volcanic rock. The median ratio of k_{sn}^E to total k_{sn} was 4.3% for reaches of sedimentary rock, and 7.2% for reaches of volcanic rock (Figures 5g, 6d).

The grain size in Ohkurasawa was significantly larger in the steeper downstream section compared to the gentler upstream section (Figure 5h). The hillslope angles also increased downstream near the lithologic boundary at approximately 1000 m, where volcanic rock began to outcrop in the upper parts of the hillslopes (Figures 1d and 7d). Upstream of this lithologic boundary, the hillslope angles did not exhibit clear variations with the rock type.

Overall, reaches of volcanic rock tend to have higher k_{sn} values than those of sedimentary rock regardless of the length of channel segment to calculate k_{sn} (Table S1). The median ratio of the residual component k_{sn}^E to total k_{sn} was only 2.4% and 4.8% in reaches of sedimentary and volcanic rock, respectively. This result indicates that the effects of the imposed sediment load could mostly explain the variation in total k_{sn} (Figure 6e, Supporting Information Table S2). Figure 6f displays the cumulative histogram of the ratio of k_{sn} components to total k_{sn} for the four rivers. The residual component k_{sn}^E accounts for a greater fraction of the total k_{sn} for the reaches of volcanic rock than that for the reaches of sedimentary rock. The difference in the fraction of k_{sn}^E between the rock type is significant in a one-sided Wilcoxon ranksum test (p = 1.9×10^{-3}; null hypothesis: the median fractions of k_{sn}^E in the reaches of sedimentary and volcanic rock are similar). The differences in the fractions of k_{sn}^E calculated using D_{50} and D_{95} are also significant ($p<0.01$; Supporting Information Figure S2). Also, while the fraction of k_{sn}^E changes with the length of channel segment used to calculate channel slope, reaches of volcanic rock always have a greater fraction of k_{sn}^E than those of sedimentary rock when the lengths of channel segment are 150, 200, and 300 m (Supporting Information Table S2).

4.3 Size and composition of bed materials

In total, I recorded sizes of 7605 grains and rock type of 6249 grains. Among the 6249 grains, 79% were of volcanic origin. The D_{50} value of volcanic rocks was 1.8 times larger than that of sedimentary rocks (Figure 8a). The D_{50} ratio between volcanic and sedimentary rocks varied across the four rivers studied—Mosawa, Shikibasawa, Yunosawa, and Ohkurasawa—with values ranging from 1.9 to 3.2 (Supporting Information Figure S3). Similarly, the D_{84} and D_{95} of volcanic rocks were larger than those of sedimentary rocks, and the magnitude of the difference between the rock types varied across the four rivers (Figures 8a and Supporting Information Figure S3). This variation suggests that the initial grain size distributions, which are supplied from hillslopes to channels, differs from one basin to another.

To explore the impact of changes in sediment source on bed material composition, I calculated the proportion of volcanic particles in each Wolman count and compared it with the proportion of volcanic rock units within the catchment area at each site (Figure 8b). The colors of the points in Figure 8b represent the ratio of the D_{84} for the volcanic and sedimentary rock particles (D_{84}^{Vol} and D_{84}^{Sed}, respectively). Despite the sampling biases associated with the Wolman count method (Bunte & Abt, 2001), which typically favor the selection of larger particles, the proportion of volcanic particles did not correlate with $D_{84}^{Vol}/D_{84}^{Sed}$ (Figure 8b). This suggests that sampling biases had minimal impact on the results. In Mosawa, where basaltic rocks occur only in the upstream half of the catchment (Figure 3), the proportion of basaltic particles in the riverbed decreases downstream as the basaltic rock units occupy a smaller area of the catchment (gray circles in Figure 8b). However, the proportion of basaltic particles remains above 64% even when basaltic rock constitutes only 45% of the upstream area, indicating an overrepresentation of basaltic gravel in the riverbed. In contrast, in the other three rivers where volcanic and sedimentary rocks are interspersed throughout the studied reach, no clear correlation was observed between the proportion of volcanic grains in the riverbed and in the catchment area, potentially because of the intermittent supply of volcanic rock.

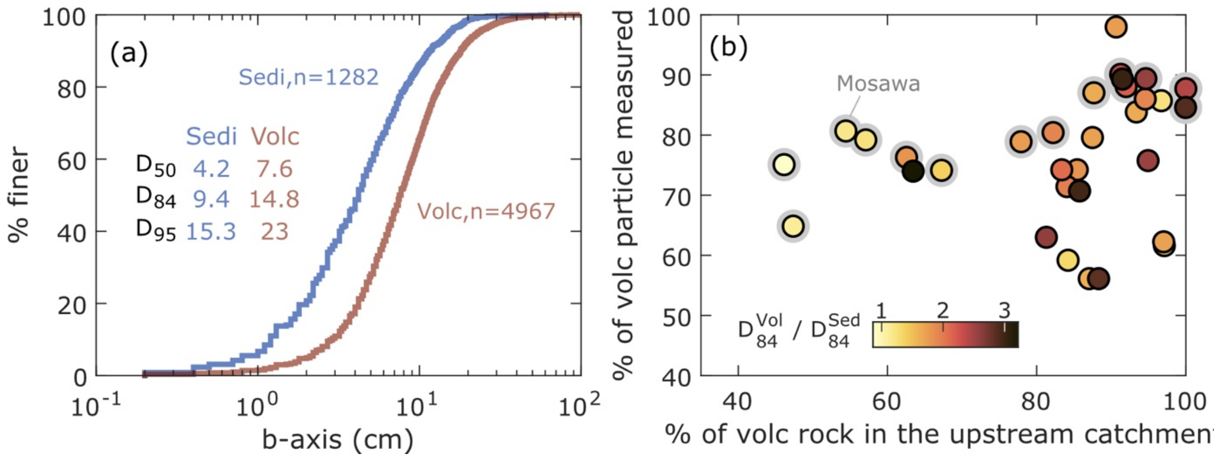

Figure 8. (a) Cumulative frequency of b-axis for particles of sedimentary and volcanic rock. (b) Effect of changing sediment source on the proportion of volcanic particles at the channel bed. The color indicates the ratio of the 84th percentile grain size for the volcanic and sedimentary rock particles measured in each Wolman count. Gray circles are data in Mosawa.

4.4 Dependency of channel width on rock type

Across all rivers, a gradual increase in channel width with drainage area was observed. The exponent b in Equation 3 varied from 0.24 to 0.47 across individual rivers, with an average value of 0.39 for the entire dataset, a typical value for mountain streams (Montgomery and Gran, 2001). Figure 9 shows channel wideness values calculated using the b value obtained in each river (Figure 9a–9e) and those calculated using the average b value of 0.39 (Figure 9f). In Tanosawa, despite larger grain sizes and higher k_{sn} values in the trunk stream Tn1 compared to the tributary Tn2, the k_w values were statistically similar between Tn1 and Tn2 as indicated by the two-sided Wilcoxon rank-sum test (Figure 9a, p = 0.54). In Mosawa and Shikibasawa, the median k_w was slightly higher in volcanic rock reaches than in sedimentary rock reaches (Figures 9b and 9c). However, these differences were not statistically significant at the 5% level in a two-sided Wilcoxon rank-sum test (p = 0.12 and 0.11 for Mosawa and Shikibasawa, respectively; the null hypothesis being that reaches of volcanic and sedimentary rock have the same median k_w values).

The median k_w in Yunosawa was larger for volcanic rock reaches than for sedimentary rock reaches (p = 0.028 in the two-sided Wilcoxon rank-sum test) (Figure 9d). Conversely, in Ohkurasawa, the median k_w was larger for sedimentary rock reaches than for volcanic rock reaches (p =0.032 in the two-sided Wilcoxon rank-sum test) (Figure 9e). Overall, no significant differences in k_w between volcanic and sedimentary rocks were found in the two-sided Wilcoxon rank-sum test (p = 0.12).

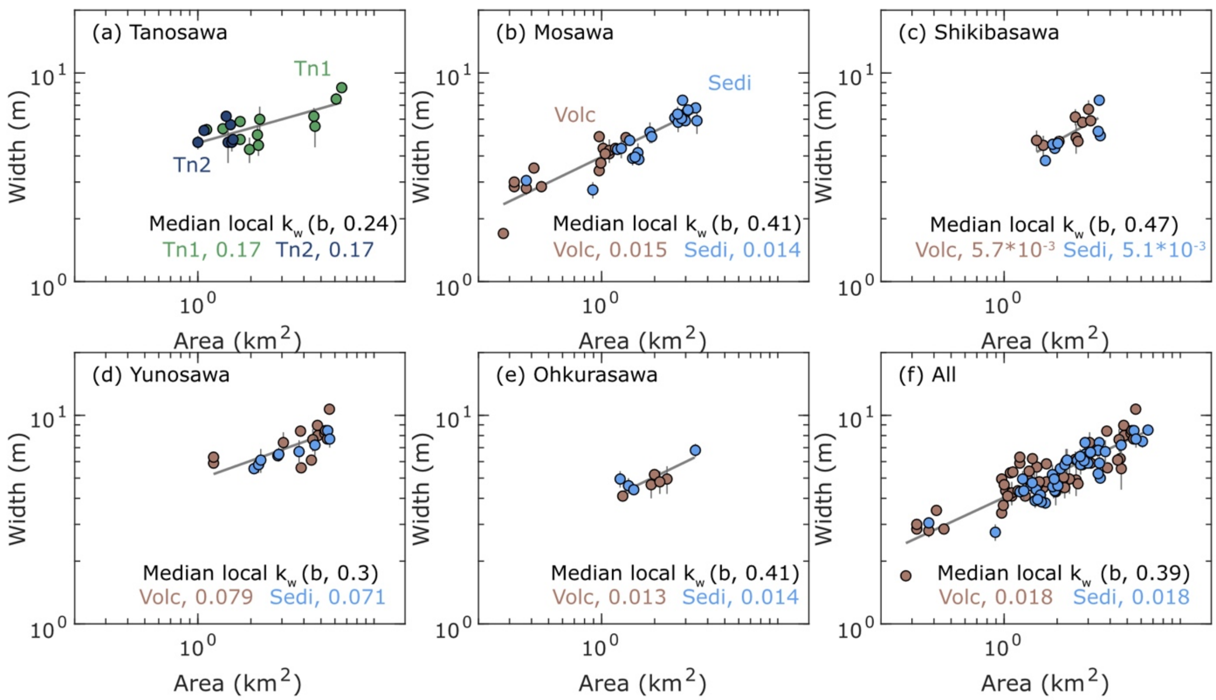

Figure 9. (a–e) Variation of channel width in each river and (f) whole study area. The exponent b in equation 3 is estimated for each river. Local wideness values k_w were calculated using the b value shown in each panel. Circles in (b–f) are colored by channel substrate.

5 Discussion

5.1 Quantifying the impact of sediment on stream profiles in mono-lithologic catchment

The analysis revealed that the difference in total k_{sn} between Tn1 and Tn2 in Tanosawa roughly corresponded to the differences in $k_{sn}^{D_s}$ and $k_{sn}^{Q_s}$ (Table 1). Given their proximity of only a few hundred meters, it is likely that Tn1 and Tn2 experienced similar climatic and tectonic forces, aligning with the observation that variations in k_{sn} predominantly resulted from sediment impacts. Although the rock erodibility may significantly differ between Tn1 and Tn2 due to heterogeneous macro- and microscopic rock properties (e.g., Turowski et al., 2023), the major cause of the contrasting profiles between Tn1 and Tn2 is argued to be the difference in grain size, as they exhibit similar k_w values and hillslope angles, which are also influenced by rock properties (Allen et al., 2013; Roda-Boluda et al., 2018). These findings in Tanosawa support the observations in the other four streams that sediment load significantly contributes to the total k_{sn} (Figures 6e and 6f).

The results of Tanosawa highlight the significance of acknowledging the spatial heterogeneity of rock properties within a geological unit and its impact on the grain size distribution in channels. Basaltic gravel constitutes 83–97% of the total gravel measured in Tanosawa, suggesting that the differences in grain size between Tn1 and Tn2 can be attributed to the initial grain size distribution of basaltic rock on hillslopes. Basaltic rocks in Tanosawa appear in various forms, including outcrops with sparse or dense joints and severe spheroidal weathering (Tsushima and Uemura, 1959; Uemura et al., 1959). Although vegetation cover limited detailed observations of the bedrock outcrops, the heterogeneity of rock properties probably caused the differences in grain size between Tn1 and Tn2. The sizes of volcanic gravel in four other streams also varied significantly (Supporting Information Figure S3), implying that the local changes in the size of volcanic gravel induced by varying degrees of fracturing, weathering, and mass movement are common in this area. Although numerous studies including the present research demonstrate that the imposed sediment load rather than rock erodibility controls the morphology of mountain rivers, the findings of this study confirm that it is also important to reveal how rock properties dictate the size and rates of sediment supply into channels (Sklar et al., 2017).

5.2 Factors that complicate the controls of rock type on channel slope

The uplift of Tsugaru Mountain, initiated in the late Pliocene due to the activity of the Tsugaru fault (Nemoto, 2014), has not been precisely dated. However, the five streams studied may still be in a transient state, as adjustments to changes in base-level fall rates can take millions of years (Whittaker et al., 2007; Yanites, 2018; Takahashi et al., 2023). A sustained increase in the rate of base-level change can create a knickpoint that propagates upstream, dividing the stream into a steeper downstream section and a gentler upstream section. After the knickpoint passes, changes in channel width (k_w) and the angles of adjacent hillslopes may occur (Whittaker et al., 2007; Hurst et al., 2012; Yanites, 2018; Baynes et al., 2022; Takahashi et al., 2023). Despite the presence of numerous knickpoints in the studied catchment, they do not correspond with changes in the reach average k_{sn} or systematic alterations in hillslope angles and k_w (Figures 3, 7, 9, and Supporting Information Figure S4). In addition, chi plots for eight stream networks draining the western flank of the Tsugaru Mountain are mostly linear (Supporting Information Figure S5), indicating their longitudinal profiles are close to those at the steady state. Therefore, it can be concluded that the transient response to changes in uplift rates has a negligible impact on interpreting the k_{sn} variations within the studied catchment.

Thereafter, I examined whether the difference in k_w between the rock types affected the variations in k_{sn}. Although the reaches of volcanic and sedimentary rocks exhibited similar k_w values in Tanosawa, Mosawa, and Shikibasawa, the reaches of volcanic rock displayed marginally larger k_w values in Yunosawa and smaller k_w values in Ohkurasawa than those of sedimentary rock (Figure 9). Generally, wider channels require steeper slopes than narrower channels to achieve equivalent incision rates.

Therefore, the differences in k_w between rock types in Yunosawa and Ohkurasawa might have influenced the observed k_{sn} values. Nonetheless, since the difference in channel width between rock types is accounted for in the slope component calculations (Equations 6 and 10) and the median k_w varies by only 10% between rock types, omitting the channel width difference does not alter the interpretation of how rock erodibility and sediment load impact channel slope.

5.3 Relative importance of rock erodibility and sediment load on setting channel slope

The slope components related to the imposed sediment load predominantly explain the variation in channel slope. This result indicates the influence of rock erodibility is considerably smaller than that of the imposed sediment load, which is consistent with the predictions from theoretical models (Sklar and Dietrich, 2006; Turowski et al., 2007). The major influence of the sediment load on channel slope relative to rock erodibility suggests that the capacity of rock to supply coarse and immobile materials into channels determines the shape of longitudinal profiles. Sediment particles from less erodible rocks are typically coarser (Roda-Boluda et al., 2018), exhibit lower mass loss rates during transport (Attal and Lavé, 2009; Bodek and Jerolmack, 2021), and are denser than those from soft rocks (Turowski et al., 2023). These characteristics contribute to the selective deposition and extended residence time of particles from less erodible rocks compared to those from erodible rocks, as suggested by the disproportionate presence of volcanic gravel in the bed relative to the areal extent of volcanic rock in the catchment (Figure 8b). Consequently, the impact of sediment load can persist even when the bedrock transitions downstream from less erodible to erodible rock types, thereby diminishing the disparity in channel steepness between different rock types (Johnson et al., 2009; Thaler and Covington, 2016; Finnegan et al., 2017; Lai et al., 2021). Thus, understanding the relationship between channel steepness and rock type necessitates an examination of how rock properties influence the sediment size supplied to channels (Sklar et al., 2017).

The predominant role of sediment load in determining channel slope complicates the assessment of a uniform response among mountain rivers in a region to changes in lithology and external conditions. Local factors such as proximity to tributary junctions, bedrock exposure along channels (Rice, 1998; Rice and Church, 1998), and heterogeneous rock properties influence the grain size distributions of bed material (DiBiase et al., 2018b; Verdian et al., 2021). The downstream evolution of grain size does not always follow the simple model (e.g., Sternberg's law) because of varied sediment sources and the mixing of rocks with different durability (Rice and Church, 1998; Attal and Lavé, 2006). Moreover, sediment dynamics can impact channel width (MacKenzie and Eaton, 2017; Baynes et al., 2020), potentially causing alterations in channel slope (Yanites, 2018). Therefore, it is reasonable that the adjustment of k_{sn} and k_w to changes in bedrock erodibility occurs in various manners on Tsugaru Mountain, where the disparity in grain size between rock types varied between catchments (Supporting Information Figure S3).

The dominance of either the tool or cover effect of sediment on erosion may dictate channel responses to changes in rock type. The erosional efficiency is influenced by the relative sediment supply (Sklar and Dietrich, 2001; Cowie et al., 2008; Scheingross et al., 2014). In a case of low relative sediment supply (tool regime), an increase in sediment supply accelerates erosion. Conversely, in a case of high relative sediment supply (cover regime), an increase in sediment supply inhibits erosion. Therefore, when a transition in rock type coincides with an increased sediment supply in the tool regime, the rivers can maintain similar erosion rates while reducing their channel slope from its original value (Sklar and Dietrich, 2004). In the cover regime, however, the channel slope must increase to counteract the increased sediment supply resulting from changes in rock type and maintain similar erosion rates across lithologic boundaries. Additionally, the temporal variations in the channel slope caused by the knickpoint passage or damming via slope failure may locally shift a reach from the cover to the tool regime or vice versa, thereby complicating the interpretation of how rock type influences channel slope. Although testing these hypotheses was beyond the scope of this study, future laboratory and numerical experiments could explore how rivers in the tool and cover regimes respond to variations in rock erodibility and sediment supply.

The layered structure of rock units with differing erodibilities can partly explain the apparent decorrelation of rock erodibility and the channel slope in Tsugaru. When bedrock incision rates are highly dependent on rock erodibility, as seen under the detachment-limited condition in the stream power model (Whipple and Tucker, 1999), differential incision across each rock unit modifies the rates of local base-level change at their interfaces (Forte et al., 2016; Perne et al., 2017). This local base-level change can lead to a steeper channel slope or slower incision in erodible rocks compared to less erodible rocks (Forte et al., 2016; Perne et al., 2017). The stratified structure was most evident at Yunosawa, where the substrate rock alternated frequently within the middle of the studied reach (Figures 1d and 3d). Unlike the four other rivers studied, k_{sn} values in the volcanic and sedimentary rocks at Yunosawa were statistically indistinguishable, potentially because of the local base-level changes caused by differential incision in the volcanic and sedimentary rocks.

The contrast of bedload erosivity and bedrock erodibility may have affected the observed variation of channel steepness. The abrasion mill experiment by Sklar and

Dietrich (2001) showed bedload composed of gravels of less erodible rock can erode bedrock faster than that composed of gravels of more erodible rock. This result indicates depending on the contrast of bedload erosivity and bedrock erodibility, the effective erodibility can deviate from the original bedrock erodibility. In that case, the difference in channel steepness between rock type can be significantly altered from the value expected from bedrock erodibility, which complicate the understanding of how rock type controls channel morphology (Fox et al., 2023; Gailleton et al., 2024; Smith et al., 2024). To evalvuate if the contrast of bedload and bedrock may affect the observed channel steepness, I compared chi plots of Mosawa and its tributary located to the south (Figure 10). In this tributary, volcanic rock occurs only in the headwaters and constitutes much smaller part of the catchment than in Mosawa (Figure 10a and 10b). Thus, the reaches of sedimentary rock in the tributary presumably receive much smaller amount of volcanic bedload than those in Mosawa, suggesting the lower effective erodibility in the tributary than in Mosawa. However, the reach average k_{sn} in sedimentary rock is similar between Mosawa and the tributary, meaning the similar effective erodibility (Figure 10c). This observation suggests the difference between bedload and bedrock materials have minor influence on channel steepness in Tsugaru. Therefore, although it is not possible to quantify the impact of bedload-bedrock contrast on the observed difference in k_{sn} between rock type, the impact can be assumed to be minor in the studied catchments.

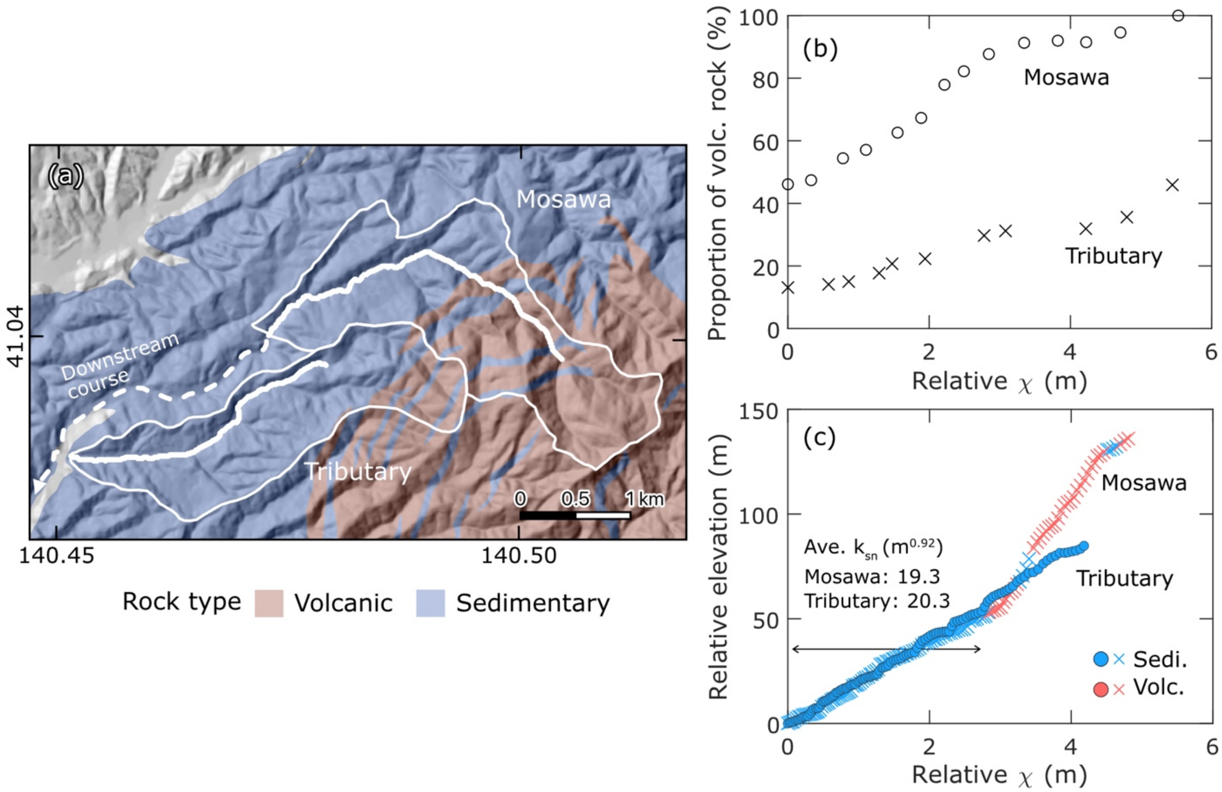

Figure 10. (a) A geologic map around Mosawa and its tributary after 1:50,000 maps (Tsushima & Uemura, 1959; Uemura et al., 1959). Stream data along the solid white lines are used in (c). (b) Proportion of volcanic rock in the upstream catchment. (c) Chi plots for Mosawa and the tributary. Color represents the type of channel substrate. Values of chi and elevation are adjusted so the most downstream point shown in (a) is plotted at the origin.

Although the channel slope is typically influenced by sediment load, the variations in rock erodibility between the rock types are evident in the study area. Waterfalls predominantly occur in volcanic rock reaches and near lithologic boundaries such as 1000–2000 m in Shikibasawa and <800 m in Ohkurasawa (Figure 3). These local increases in k_{sn} did not correspond to the abrupt changes in hillslope angles or tributary junctions, indicating minor variations in sediment supply. Also, bedrock exposure was more extensive in these steep reaches than adjacent gentler reaches. Thus, these local highs of k_{sn} are probably attributable to low rock erodibility. This interpretation is supported by the model predictions of Guryan et al. (2024), who employed a modified version of the stream power model incorporating the conservation and transport of eroded mass (Shobe et al., 2017). They found that when the sediment supply remains relatively constant, channel slope becomes higher in rocks of lower erodibility, leading to greater sediment entrainment rates. Consequently, sediment cover decreases in areas of low bedrock erodibility. The saltation-abrasion model predicts similar responses of channel slope and the degree of bedrock exposure to an increase in rock tensile strength (Sklar and Dietrich, 2006). Investigating these steeper reaches with thinner alluvial cover could reveal the conditions under which the influence of rock erodibility on channel slope outweighs that of the imposed sediment load. However, studying such steep reaches was impractical, as they were exceedingly steep to traverse and lacked subaerial bars necessary for measuring more than 100 grains.

Lastly, it is important to note slope component analysis cannot reveal how bedrock erosion occurs at the same rates across rocks of different erodibility. When a channel is steeper in less erodible rock than in erodible rock, the differential erodibility may be offset by the difference in the degree of bedrock exposure (Sklar and Dietrich, 2006; Guryan et al., 2024). However, if channel slope is similar between reaches of different bedrock erodibility, it is unclear why and whether erosion rates are kept similar between those reaches. According to the saltation abrasion model, slight change in channel slope can significantly reduce the alluvial cover over rocks of lower erodibility, keeping erosion rate in less erodible rock similar to that in erodible rock (Sklar and Dietrich, 2006). If this is the case, although the same erosion rates may be achieved, it would be difficult to detect such small changes in channel slope of natural rivers.

Another possibility is the difference in erosional efficiency due to the contrast of bedload and bedrock erodibility (Sklar and Dietrich, 2001; Fox et al., 2023) or erosion process (Whipple et al., 2000; Chatanantabet and Parker, 2009; Lamb et al., 2015). In Tsugaru, the effect of bedload-bedrock contrast is not apparent at least in the channel profiles (Figure 10). For erosion process, erosion by plucking may be more dominant in volcanic rocks than in sedimentary rocks in Tsugaru. In particular, volcanic bedrock often exhibited rugged surface on channel walls, suggesting lateral erosion rates and the adjustment of channel width to changes in the boundary conditions are different between rock type. However, the surface of volcanic rocks exposed at riverbed was generally smooth. Also, sedimentary rocks in the study area are composed of beds that are blocky and prone to plucking and those that are very smooth and likely eroded by frictional abrasion. Thus, it was hard to determine if the dominant erosion process clearly differs by rock type. If none of the above applies, it may be necessary to consider cases where the topographic steady state is not achieved due to different vertical erosion rates in different rock types (Forte et al., 2016; Perne et al., 2017).

5.4 Limitations in the slope component analysis

Slope component analysis is a valuable method for quantifying the contributions of imposed sediment load to longitudinal stream profiles using field-measurable parameters (Sklar & Dietrich, 2006; Lai et al., 2021). However, certain parameters required for this analysis are not easily measurable in the field and depend on the selection of theoretical or empirical equations. This section addresses the challenges in calculating S_{D_s} and ΔS_{Q_s} and provide their minimum estimates.

A primary concern is the entrainment threshold, τ_c^*. I adopted τ_c^* proposed by Lamb et al. (2008), which is a simple function of channel slope. This threshold is practical for field studies and is applicable to headwater streams, as it is derived from both flume and field data encompassing a channel slope up to 0.2, typical of headwaters.

Nonetheless, accurate estimation of τ_c^* has proven extremely challenging (Buffington & Montgomery, 1997; Petit et al., 2015; Phillips et al., 2022; Perret et al., 2023; Hodge et al., 2024). Among the various factors causing spatial and temporal variations in τ_c^*, grain protrusion is arguably the most significant when calculating the slope component related to the entrainment threshold (S_{D_s}). Coarser grains in a given grain size distribution tend to protrude from the bed, exposing a larger area to the flow. This modifies τ_c^* based on the protruded height of the grain relative to D_{50} (Hodge et al., 2020; Smith et al., 2023), significantly reducing τ_c^* for grains sized D_{84} compared to the value predicted by Equation 9, which is based on the median-sized grains (Lamb et al., 2008).

Despite these complexities, I argue that the slope component S_{D_s} remains critical because the residence time of gravel in the channel is influenced by both the frequency of entrainment and the transport distance. Vázquez-Tarrío et al. (2019) has compiled published data on gravel transport using passive tracers. Their findings reveal that the transport distance of gravel decreases exponentially with size relative to the median grain size. Furthermore, once a large grain on the bar is entrained, the bed roughness decreases, and the grains previously sheltered by the entrained grain become more mobile. Therefore, although estimates of S_{D_s} may vary significantly when accounting for grain protrusion, the impact is mitigated by the exponential reduction in transport distance with size and the reorganization of the bed following the entrainment of coarse grains.

Quantifying the relative sediment supply from the degree of exposed bedrock (Equation 11) presents a significant challenge. Flume experiments conducted by Chatanantavet and Parker (2008) demonstrated that F_e either linearly decreased with an increase in the relative sediment supply or abruptly dropped from 1 (fully exposed) to 0 (no exposure). Subsequent studies confirmed both gradual and abrupt alluviation (Johnson & Whipple, 2010; Inoue et al., 2014; Mishra & Inoue, 2020; Cho & Nelson, 2024), and the rate of change in F_e with the increasing relative sediment supply is much more diverse than predicted by Equation 11, partly due to the relative surface roughness of the alluvial cover and bedrock (Mishra & Inoue, 2020). However, owing to the lack of constraints on the roughness of the bedrock, discussing the uncertainty in the relative sediment supply was not possible in this study.

The difficulties with accurate constraints on S_{D_s} and ΔS_{Q_S} indicate that their minimum estimates can be presented to ensure the validity of the present findings. For S_{D_s}, I used τ_c^* =0.02, which is roughly one-third of the values predicted by Lamb et al. (2008) and in the smallest range reported in previous studies (Buffiington & Montgomery, 1997; Petit et al., 2015; Perret et al., 2023). For ΔS_{Q_S}, I set F_e=0.7 for all sites, the minimum value observed in Tsugaru (Figure 5) and used $\frac{Q_s}{Q_c}$=0.3, which is generally lower than the values predicted by the existing models (Mishra & Inoue, 2020). Except for τ_c^* and $\frac{Q_s}{Q_c}$, I used the same parameters as those used to calculate S_{D_s} and ΔS_{Q_S} displayed in Figure 5. The resulting sum of S_{D_s} and ΔS_{Q_S} was 54% of total slope on average and ranged 47–132% of total slope. Therefore, I can reasonably conclude that the imposed sediment load controls the channel slope more strongly than rock erodibility.

6 Conclusions

The minimum channel slope required to transport the imposed sediment load for five rivers in the Tsugaru Mountain region were calculated to determine that the sediment load generally exerts a stronger influence on channel slope than rock erodibility. This finding persists even when using very small values for the threshold of incipient motion and relative sediment supply to estimate sediment effects. Additionally, the locally steepened reaches with the thinner alluvial cover possibly resulted from contrasts in erodibility, which is consistent with previous model predictions. These observations confirm that rock erodibility influences stream profiles by modulating erosional resistance and the mobility of rock particles. They suggest that future studies should investigate the conditions under which the effects of rock erodibility outweigh the impact of sediment load. The slope component analysis facilitates the quantification of sediment impact, which is challenging to estimate in the field. However, it is important to acknowledge that the uncertainty in the results could not be evaluated easily due to difficulties in constraining the entrainment threshold and relative sediment supply.

REFERENCES

Allen, G. H., Barnes, J. B., Pavelsky, T. M., & Kirby, E. (2013). Lithologic and tectonic controls on bedrock channel form at the northwest Himalayan front. *Journal of Geophysical Research: Earth Surface*, *118*(3), 1806–1825. https://doi.org/10.1002/jgrf.20113

Anderson, S., Gasparini, N., & Johnson, J. (2023). Building a bimodal landscape: Bedrock lithology and bed thickness controls on the morphology of Last Chance Canyon, New Mexico, USA. *Earth Surface*

Dynamics, *11*(5), 995–1011. https://doi.org/10.5194/esurf-11-995-2023

Attal, M., & Lavé, J. (2006). Changes of bedload characteristics along the Marsyandi River (central Nepal): Implications for understanding hillslope sediment supply, sediment load evolution along fluvial networks, and denudation in active orogenic belts. In S. D. Willett, N. Hovius, M. T. Brandon, & D. M. Fisher, *Tectonics, Climate, and Landscape Evolution*. Geological Society of America. https://doi.org/10.1130/2006.2398(09)

Attal, M., & Lavé, J. (2009). Pebble abrasion during fluvial transport: Experimental results and implications for the evolution of the sediment load along rivers. *Journal of Geophysical Research: Earth Surface*, *114*(F4), 2009JF001328. https://doi.org/10.1029/2009JF001328

Baynes, E. R. C., Lague, D., Steer, P., Bonnet, S., & Illien, L. (2020). Sediment flux-driven channel geometry adjustment of bedrock and mixed gravel–bedrock rivers. *Earth Surface Processes and Landforms*, *45*(14), 3714–3731. https://doi.org/10.1002/esp.4996

Baynes, E. R. C., Lague, D., Steer, P., & Davy, P. (2022). Dynamic bedrock channel width during knickpoint retreat enhances undercutting of coupled hillslopes. *Earth Surface Processes and Landforms*, *47*(15), 3629–3640. https://doi.org/10.1002/esp.5477

Bodek, S., & Jerolmack, D. J. (2021). Breaking down chipping and fragmentation in sediment transport: The control of material strength.

Earth Surface Dynamics, *9*(6), 1531–1543. https://doi.org/10.5194/esurf-9-1531-2021

Buffington, J. M., & Montgomery, D. R. (1997). A systematic analysis of eight decades of incipient motion studies, with special reference to gravel-bedded rivers. *Water Resources Research*, *33*(8), 1993–2029. https://doi.org/10.1029/96WR03190

Bunte, K., & Abt, S. R. (2001). *Sampling surface and subsurface particle-size distributions in wadable gravel-and cobble-bed streams for analyses in sediment transport, hydraulics, and streambed monitoring.* RMRS-GTR-74. U.S. Department of Agriculture, Forest Service, Rocky Mountain Research Station. https://doi.org/10.2737/RMRS-GTR-74

Bursztyn, N., Pederson, J. L., Tressler, C., Mackley, R. D., & Mitchell, K. J. (2015). Rock strength along a fluvial transect of the Colorado Plateau – quantifying a fundamental control on geomorphology. *Earth and Planetary Science Letters*, *429*, 90–100. https://doi.org/10.1016/j.epsl.2015.07.042

Carr, J. C., DiBiase, R. A., Yeh, E.-C., Fisher, D. M., & Kirby, E. (2023). Rock properties and sediment caliber govern bedrock river morphology across the Taiwan Central Range. *Science Advances*, *9*(46), eadg6794. https://doi.org/10.1126/sciadv.adg6794

Chatanantavet, P., & Parker, G. (2008). Experimental study of bedrock channel alluviation under varied sediment supply and hydraulic conditions. *Water Resources Research*, *44*(12), 2007WR006581. https://doi.org/10.1029/2007WR006581

Chatanantavet, P., & Parker, G. (2009). Physically based modeling of bedrock incision by abrasion, plucking, and macroabrasion. *Journal of Geophysical Research: Earth Surface*, *114*(F4), 2008JF001044. https://doi.org/10.1029/2008JF001044

Cho, J., & Nelson, P. A. (2024). Patterns of Alluviation in Mixed Bedrock-Alluvial Channels: 2. Controls on the Formation of Alluvial Patches. *Journal of Geophysical Research: Earth Surface*, *129*(1), e2023JF007293. https://doi.org/10.1029/2023JF007293

Cowie, P. A., Whittaker, A. C., Attal, M., Roberts, G., Tucker, G. E., & Ganas, A. (2008). New constraints on sediment-flux–dependent river incision: Implications for extracting tectonic signals from river profiles. *Geology*, *36*(7), 535. https://doi.org/10.1130/G24681A.1

Crameri, F. (2018). Scientific colour maps, Zenodo, doi:10.5281/zenodo.1243862

DiBiase, R. A., Denn, A. R., Bierman, P. R., Kirby, E., West, N., & Hidy, A. J. (2018a). Stratigraphic control of landscape response to base-level fall, Young Womans Creek, Pennsylvania, USA. *Earth and Planetary Science Letters*, *504*, 163–173. https://doi.org/10.1016/j.epsl.2018.10.005

DiBiase, R. A., Rossi, M. W., & Neely, A. B. (2018b). Fracture density and grain size controls on the relief structure of bedrock landscapes. *Geology*, *46*(5), 399–402. https://doi.org/10.1130/G40006.1

Duvall, A., Kirby, E., & Burbank, D. (2004). Tectonic and lithologic controls on bedrock channel profiles and processes in coastal California. *Journal of Geophysical Research: Earth Surface*, *109*(F3), 2003JF000086. https://doi.org/10.1029/2003JF000086

Fernandez-Luque, R. & van Beek, R. (1976) Erosion and transport of bed-load sediment. *Journal of Hydraulic Research*, 14, 127–144. https://doi.org/10.1080/00221687609499677

Finnegan, N. J., Klier, R. A., Johnstone, S., Pfeiffer, A. M., & Johnson, K. (2017). Field evidence for the control of grain size and sediment supply on steady-state bedrock river channel slopes in a tectonically active setting. *Earth Surface Processes and Landforms*, *42*(14), 2338–2349. https://doi.org/10.1002/esp.4187

Forte, A. M., Yanites, B. J., & Whipple, K. X. (2016). Complexities of landscape evolution during incision through layered stratigraphy with contrasts in rock strength. *Earth Surface Processes and Landforms*, *41*(12), 1736–1757. https://doi.org/10.1002/esp.3947

Fox, M., Hoseason, T., Bernard, T., Sinclair, H., & Smith, A. G. G. (2023). Bedload-Bedrock Contrasts Form Enigmatic Low-Relief Surfaces of the

Pyrenees. *Geophysical Research Letters*, *50*(6), e2022GL101995. https://doi.org/10.1029/2022GL101995

Fujii, K. (1981) Geology of the Abukuma District. Quadrangle Series, Scale 1:50,000, Geological Survey of Japan, 38p.

Gailleton, B., Malatesta, L. C., Cordonnier, G., & Braun, J. (2024). CHONK 1.0: Landscape evolution framework: cellular automata meets graph theory. *Geoscientific Model Development*, *17*(1), 71–90. https://doi.org/10.5194/gmd-17-71-2024

Gallen, S. F. (2018). Lithologic controls on landscape dynamics and aquatic species evolution in post-orogenic mountains. *Earth and Planetary Science Letters*, *493*, 150–160. https://doi.org/10.1016/j.epsl.2018.04.029

Geological Survey of Japan, AIST (2023) Seamless digital geological map of Japan V2 1:200,000, Original edition. https://gbank.gsj.jp/seamless/ [Accessed: Jul. 20th, 2024]

Guryan, G. J., Johnson, J. P. L., & Gasparini, N. M. (2024). Sediment Cover Modulates Landscape Erosion Patterns and Channel Steepness in Layered Rocks: Insights From the SPACE Model. *Journal of Geophysical Research: Earth Surface*, *129*(7), e2023JF007509.https://doi.org/10.1029/2023JF007509

Hack, J.T. (1957) Studies of Longitudinal Stream Profiles in Virginia and Maryland. *United States Geological Survey Professional paper*, 294-B, 45–97. https://doi.org/10.3133/pp294B

Hack, J.T. (1973) Stream-profile analysis and stream-gradient index. *Journal of Research of the U. S. Geological Survey*, 1(4), 421–429.

Harel, M.-A., Mudd, S. M., & Attal, M. (2016). Global analysis of the stream power law parameters based on worldwide 10Be denudation rates. *Geomorphology*, *268*, 184–196. https://doi.org/10.1016/j.geomorph.2016.05.035

The headquarters for earthquake research promotion (2004) On the long-term evaluation of the western marginal fault zone of the Aomori bay. https://www.jishin.go.jp/main/chousa/katsudansou_pdf/09_aomori-wan.pdf [Accessed:Aug. 15th, 2024]

Hodge, R. A., Voepel, H., Leyland, J., Sear, D. A., & Ahmed, S. (2020). X-ray computed tomography reveals that grain protrusion controls critical shear stress for entrainment of fluvial gravels. *Geology*, *48*(2), 149–153. https://doi.org/10.1130/G46883.1

Hodge, R. A., Voepel, H. E., Yager, E. M., Leyland, J., Johnson, J. P. L., Sear, D. A., & Ahmed, S. (2024). Improving predictions of critical shear stress in gravel bed rivers: Identifying the onset of sediment transport and quantifying sediment structure. *Earth Surface Processes and Landforms*, *49*(8), 2517–2537. https://doi.org/10.1002/esp.5842

Howard, A. D., & Kerby, G. (1983). Channel changes in badlands. *Geological Society of America Bulletin*, *94*(6), 739. https://doi.org/10.1130/0016-7606(1983)94<739:CCIB>2.0.CO;2

Hurst, M. D., Mudd, S. M., Walcott, R., Attal, M., & Yoo, K. (2012). Using hilltop curvature to derive the spatial distribution of erosion rates. *Journal of Geophysical Research: Earth Surface*, *117*(F2), 2011JF002057. https://doi.org/10.1029/2011JF002057

Inoue, T., Izumi, N., Shimizu, Y., & Parker, G. (2014). Interaction among alluvial cover, bed roughness, and incision rate in purely bedrock and alluvial-bedrock channel. *Journal of Geophysical Research: Earth Surface*, *119*(10), 2123–2146. https://doi.org/10.1002/2014JF003133

Johnson, J. P. L., Whipple, K. X., Sklar, L. S., & Hanks, T. C. (2009). Transport slopes, sediment cover, and bedrock channel incision in the Henry Mountains, Utah. *Journal of Geophysical Research: Earth Surface*, *114*(F2), 2007JF000862. https://doi.org/10.1029/2007JF000862

Johnson, J. P. L., & Whipple, K. X. (2010). Evaluating the controls of shear stress, sediment supply, alluvial cover, and channel morphology on experimental bedrock incision rate. *Journal of Geophysical Research: Earth Surface*, *115*(F2), 2009JF001335. https://doi.org/10.1029/2009JF001335

Kirby, E., Whipple, K. X., Tang, W., & Chen, Z. (2003). Distribution of active rock uplift along the eastern margin of the Tibetan Plateau: Inferences from bedrock channel longitudinal profiles. *Journal of Geophysical Research: Solid Earth*, *108*(B4), 2001JB000861. https://doi.org/10.1029/2001JB000861

Lai, L. S., Roering, J. J., Finnegan, N. J., Dorsey, R. J., & Yen, J. (2021). Coarse sediment supply sets the slope of bedrock channels in rapidly uplifting terrain: Field and topographic evidence from eastern Taiwan. *Earth Surface Processes and Landforms*, *46*(13), 2671–2689. https://doi.org/10.1002/esp.5200

Lamb, M. P., Dietrich, W. E., & Venditti, J. G. (2008). Is the critical Shields stress for incipient sediment motion dependent on channel-bed slope? *Journal of Geophysical Research: Earth Surface*, *113*(F2), 2007JF000831. https://doi.org/10.1029/2007JF000831

Lamb, M. P., Finnegan, N. J., Scheingross, J. S., & Sklar, L. S. (2015). New insights into the mechanics of fluvial bedrock erosion through flume experiments and theory. *Geomorphology*, *244*, 33–55. https://doi.org/10.1016/j.geomorph.2015.03.003

Leonard, J. S., Whipple, K. X., & Heimsath, A. M. (2023). Isolating climatic, tectonic, and lithologic controls on mountain landscape evolution. *Science Advances*, *9*(3), eadd8915. https://doi.org/10.1126/sciadv.add8915

MacKenzie, L. G., & Eaton, B. C. (2017). Large grains matter: Contrasting bed stability and morphodynamics during two nearly identical experiments. *Earth Surface Processes and Landforms*, *42*(8), 1287–1295. https://doi.org/10.1002/esp.4122

MacKenzie, L. G., Eaton, B. C., & Church, M. (2018). Breaking from the average: Why large grains matter in gravel-bed streams. *Earth Surface Processes and Landforms*, *43*(15), 3190–3196. https://doi.org/10.1002/esp.4465

Mimura, T. (1979) On the development of the geological structure in the southern part of the Tsugaru peninsula, Aomori Prefecture. *Journal of Geological Society of Japan*, 85(12), 719–735. https://doi.org/10.5575/geosoc.85.719

Mishra, J., & Inoue, T. (2020). Alluvial cover on bedrock channels: Applicability of existing models. *Earth Surface Dynamics*, *8*(3), 695–716. https://doi.org/10.5194/esurf-8-695-2020

Molnar, P., Anderson, R. S., & Anderson, S. P. (2007). Tectonics, fracturing of rock, and erosion. *Journal of Geophysical Research: Earth Surface*, *112*(F3), 2005JF000433. https://doi.org/10.1029/2005JF000433

Montgomery, D. R., & Gran, K. B. (2001). Downstream variations in the width of bedrock channels. *Water Resources Research*, *37*(6), 1841–1846. https://doi.org/10.1029/2000WR900393

Montgomery, D. R., & Brandon, M. T. (2002). Topographic controls on erosion rates in tectonically active mountain ranges. *Earth and

Planetary Science Letters, *201*(3–4), 481–489. https://doi.org/10.1016/S0012-821X(02)00725-2

Nakata, T. & Imaizumi, T. (Eds.) (2002) Digital active fault map of Japan. University of Tokyo press.

Nemoto, N. (2014) Neogene to Quaternary tectonics in the Tsugaru Peninsula, northeast Japan. *The Quaternary Research*, 53(4), 205–212. https://doi.org/10.4116/jaqua.53.205

Perne, M., Covington, M. D., Thaler, E. A., & Myre, J. M. (2017). Steady state, erosional continuity, and the topography of landscapes developed in layered rocks. *Earth Surface Dynamics*, *5*(1), 85–100. https://doi.org/10.5194/esurf-5-85-2017

Perret, E., Camenen, B., Berni, C., El Kadi Abderrezzak, K., & Renard, B. (2023). Uncertainties in Models Predicting Critical Bed Shear Stress of Cohesionless Particles. *Journal of Hydraulic Engineering*, *149*(4), 04023002. https://doi.org/10.1061/JHEND8.HYENG-13101

Perron, J. T., & Royden, L. (2013). An integral approach to bedrock river profile analysis. *Earth Surface Processes and Landforms*, *38*(6), 570–576. https://doi.org/10.1002/esp.3302

Petit, F., Houbrechts, G., Peeters, A., Hallot, E., Van Campenhout, J., & Denis, A.-C. (2015). Dimensionless critical shear stress in gravel-bed rivers. *Geomorphology*, *250*, 308–320. https://doi.org/10.1016/j.geomorph.2015.09.008

Phillips, C. B., Masteller, C. C., Slater, L. J., Dunne, K. B. J., Francalanci, S., Lanzoni, S., Merritts, D. J., Lajeunesse, E., & Jerolmack, D. J. (2022). Threshold constraints on the size, shape and stability of alluvial rivers. *Nature Reviews Earth & Environment*, *3*(6), 406–419. https://doi.org/10.1038/s43017-022-00282-z

Rice, S. (1998). Which tributaries disrupt downstream fining along gravel-bed rivers? *Geomorphology*, *22*(1), 39–56. https://doi.org/10.1016/S0169-555X(97)00052-4

Rice, S., & Church, M. (1998). Grain size along two gravel-bed rivers: Statistical variation, spatial pattern and sedimentary links. *Earth Surface Processes and Landforms*, *23*(4), 345–363. https://doi.org/10.1002/(SICI)1096-9837(199804)23:4<345::AID-ESP850>3.0.CO;2-B

Roda-Boluda, D. C., D'Arcy, M., McDonald, J., & Whittaker, A. C. (2018). Lithological controls on hillslope sediment supply: Insights from landslide activity and grain size distributions. *Earth Surface Processes and Landforms*, *43*(5), 956–977. https://doi.org/10.1002/esp.4281

Roering, J. J., Kirchner, J. W., & Dietrich, W. E. (2001). Hillslope evolution by nonlinear, slope-dependent transport: Steady state morphology and equilibrium adjustment timescales. *Journal of Geophysical Research: Solid Earth*, *106*(B8), 16499–16513. https://doi.org/10.1029/2001JB000323

Scheingross, J. S., Brun, F., Lo, D. Y., Omerdin, K., & Lamb, M. P. (2014). Experimental evidence for fluvial bedrock incision by suspended and bedload sediment. *Geology*, *42*(6), 523–526. https://doi.org/10.1130/G35432.1

Schwanghart, W., & Scherler, D. (2014). Short Communication: TopoToolbox 2 – MATLAB-based software for topographic analysis and modeling in Earth surface sciences. *Earth Surface Dynamics*, *2*(1), 1–7. https://doi.org/10.5194/esurf-2-1-2014

Shobe, C. M., Tucker, G. E., & Barnhart, K. R. (2017). The SPACE 1.0 model: A Landlab component for 2-D calculation of sediment transport, bedrock erosion, and landscape evolution. *Geoscientific Model Development*, *10*(12), 4577–4604. https://doi.org/10.5194/gmd-10-4577-2017

Shobe, C. M., Bennett, G. L., Tucker, G. E., Roback, K., Miller, S. R., & Roering, J. J. (2021a). Boulders as a lithologic control on river and landscape response to tectonic forcing at the Mendocino triple junction. *GSA Bulletin*, *133*(3–4), 647–662. https://doi.org/10.1130/B35385.1

Shobe, C. M., Turowski, J. M., Nativ, R., Glade, R. C., Bennett, G. L., & Dini, B. (2021b). The role of infrequently mobile boulders in modulating landscape evolution and geomorphic hazards. *Earth-Science Reviews*, *220*, 103717. https://doi.org/10.1016/j.earscirev.2021.103717

Sklar, L. S., & Dietrich, W. E. (2001). Sediment and rock strength controls on river incision into bedrock. *Geology*, *29*(12), 1087. https://doi.org/10.1130/0091-7613(2001)029<1087:SARSCO>2.0.CO;2

Sklar, L. S., & Dietrich, W. E. (2004). A mechanistic model for river incision into bedrock by saltating bed load. *Water Resources Research*, *40*(6), 2003WR002496. https://doi.org/10.1029/2003WR002496

Sklar, L. S., & Dietrich, W. E. (2006). The role of sediment in controlling steady-state bedrock channel slope: Implications of the saltation–abrasion incision model. *Geomorphology*, *82*(1–2), 58–83. https://doi.org/10.1016/j.geomorph.2005.08.019

Sklar, L. S., Riebe, C. S., Marshall, J. A., Genetti, J., Leclere, S., Lukens, C. L., & Merces, V. (2017). The problem of predicting the size distribution of sediment supplied by hillslopes to rivers. *Geomorphology*, *277*, 31–49. https://doi.org/10.1016/j.geomorph.2016.05.005

Sklar, L. S. (2024). Grain Size in Landscapes. *Annual Review of Earth and Planetary Sciences*, *52*(1), 663–692. https://doi.org/10.1146/annurev-earth-052623-075856

Smith, H. E. J., Monsalve, A. D., Turowski, J. M., Rickenmann, D., & Yager, E. M. (2023). Controls of local grain size distribution, bed structure and flow conditions on sediment mobility. *Earth Surface Processes and Landforms*, *48*(10), 1990–2004. https://doi.org/10.1002/esp.5599

Smith, A. G. G., Fox, M., Moore, J. R., Miller, S. R., Goren, L., Morriss, M. C., & Carter, A. (2024). One Million Years of Climate-Driven Rock Uplift Rate Variation on the Wasatch Fault Revealed by Fluvial Topography. *American Journal of Science*, *324*. https://doi.org/10.2475/001c.92194

Snyder, N. P. (2000). Landscape response to tectonic forcing: Digital elevation model analysis of stream profiles in the Mendocino triple junction region, northern California. *Geological Society of America Bulletin*.

Stock, J., & Dietrich, W. E. (2003). Valley incision by debris flows: Evidence of a topographic signature. *Water Resources Research*, *39*(4), 2001WR001057. https://doi.org/10.1029/2001WR001057

Suzuki, T., Eden, D., Danhara, T., & Fujiwara, O. (2005). Correlation of the Hakkoda–Kokumoto Tephra, a widespread Middle Pleistocene tephra erupted from the Hakkoda Caldera, northeast Japan. *Island Arc*, *14*(4), 666–678. https://doi.org/10.1111/j.1440-1738.2005.00475.x

Takahashi, N., Shyu, J. B. H., Chen, C.-Y., & Toda, S. (2022). Long-term uplift pattern recorded by rivers across contrasting lithology: Insights into earthquake recurrence in the epicentral area of the 2016 Kumamoto earthquake, Japan. *Geomorphology*, *419*, 108492. https://doi.org/10.1016/j.geomorph.2022.108492

Takahashi, N. O., Shyu, J. B. H., Toda, S., Matsushi, Y., Ohta, R. J., & Matsuzaki, H. (2023). Transient Response and Adjustment Timescales of Channel Width and Angle of Valley-Side Slopes to Accelerated Incision. *Journal of Geophysical Research: Earth Surface*, *128*(8), e2022JF006967. https://doi.org/10.1029/2022JF006967

Thaler, E. A., & Covington, M. D. (2016). The influence of sandstone caprock material on bedrock channel steepness within a tectonically passive setting: Buffalo National River Basin, Arkansas, USA. *Journal of Geophysical Research: Earth Surface*, *121*(9), 1635–1650. https://doi.org/10.1002/2015JF003771

Tsushima, K. & Uemura, F. (1959) Explanatory text of the geological map of Japan, Scale 1:50000, Kodomari. Geological Survey of Japan, 43p.

Turowski, J. M., Lague, D., & Hovius, N. (2007). Cover effect in bedrock abrasion: A new derivation and its implications for the modeling of bedrock channel morphology. *Journal of Geophysical Research: Earth Surface*, *112*(F4), 2006JF000697. https://doi.org/10.1029/2006JF000697

Turowski, J. M., Pruß, G., Voigtländer, A., Ludwig, A., Landgraf, A., Kober, F., & Bonnelye, A. (2023). Geotechnical controls on erodibility in fluvial impact erosion. *Earth Surface Dynamics*, *11*(5), 979–994. https://doi.org/10.5194/esurf-11-979-2023

Uemura, F. (1959) Explanatory text of the geological map of Japan, Scale 1:50000, Kodomari. Geological Survey of Japan, 39p.

Ujiie, Y., Taniguchi, T., Ebina, M. (2006) Evaluation of the displacement of the Tsugaru Fault by means of organic maturity of fossil pollen in sediments. *Journal of Geological Society of Japan*, 112(10), 581–593. https://doi.org/10.5575/geosoc.112.581

Vázquez-Tarrío, D., Recking, A., Liébault, F., Tal, M., & Menéndez-Duarte, R. (2019). Particle transport in gravel-bed rivers: Revisiting passive tracer data. *Earth Surface Processes and Landforms*, *44*(1), 112–128. https://doi.org/10.1002/esp.4484

Verdian, J. P., Sklar, L. S., Riebe, C. S., & Moore, J. R. (2021). Sediment size on talus slopes correlates with fracture spacing on bedrock cliffs: Implications for predicting initial sediment size distributions on hillslopes. *Earth Surface Dynamics*, *9*(4), 1073–1090. https://doi.org/10.5194/esurf-9-1073-2021

Whipple, K. X., & Tucker, G. E. (1999). Dynamics of the stream-power river incision model: Implications for height limits of mountain ranges, landscape response timescales, and research needs. *Journal of Geophysical Research: Solid Earth*, *104*(B8), 17661–17674. https://doi.org/10.1029/1999JB900120

Whipple, K. X., Hancock, G. S., & Anderson, R. S. (2000). River incision into bedrock: Mechanics and relative efficacy of plucking, abrasion, and cavitation. *Geological Society of America Bulletin*, *112*(3), 490–503. https://doi.org/10.1130/0016-7606(2000)112<490:RIIBMA>2.0.CO;2

Whipple, K. X., & Tucker, G. E. (2002). Implications of sediment-flux-dependent river incision models for landscape evolution. *Journal of Geophysical Research: Solid Earth*, *107*(B2). https://doi.org/10.1029/2000JB000044

Whittaker, A. C., Cowie, P. A., Attal, M., Tucker, G. E., & Roberts, G. P. (2007). Contrasting transient and steady-state rivers crossing active normal faults: New field observations from the Central Apennines, Italy. *Basin Research*, *19*(4), 529–556. https://doi.org/10.1111/j.1365-2117.2007.00337.x

Yanites, B. J. (2018). The Dynamics of Channel Slope, Width, and Sediment in Actively Eroding Bedrock River Systems. *Journal of Geophysical Research: Earth Surface*, *123*(7), 1504–1527. https://doi.org/10.1029/2017JF004405

Yanites, B. J., Becker, J. K., Madritsch, H., Schnellmann, M., & Ehlers, T. A. (2017). Lithologic Effects on Landscape Response to Base Level Changes: A Modeling Study in the Context of the Eastern Jura Mountains, Switzerland. *Journal of Geophysical Research: Earth Surface*, *122*(11), 2196–2222. https://doi.org/10.1002/2016JF004101

Figure captions

Figure 1. Geology of the study area. Faults and active faults are after Geological survey of Japan (2023) and Nakata and Imaizumi (2002), respectively. (a) Geologic map is modified after a 1:200,000 map (Geological survey of Japan, 2023). Inset shows the location of the Tsugaru Mountain. (b–d) River sections and their catchment areas investigated in this study. Geologic map is modified after 1:50,000 maps (Tsushima & Uemura, 1959; Uemura et al., 1959; Fujii, 1981).

Figure 2. Bedrock outcrops of basalt in Shikibasawa. (a) Densely jointed bedrock exposed in a stream channel. Length of hammer: ~30 cm. (b) Bedrock outcrop with minor surficial cracks.

Figure 3. Longitudinal profiles (lines) and normalized channel steepness (circles) along the studied sections. Bar at the top represents channel substrate. (a) Blue and green circles represent normalized channel steepness of the trunk stream (Tn1) and the tributary (Tn2). Blue and green lines are stream profiles of Tn1 and Tn2.

Figure 4. Comparison of k_{sn} components and total k_{sn} in Tanosawa.

Figure 5. Variation of each k_{sn} component and key factors associated with the imposed sediment load. The top bar in (a), (c), (e), and (g) represents channel substrate.

Figure 6. Comparison of k_{sn} components and total k_{sn} for volcanic and sedimentary rock. Results of (a-d) the individual rivers and (e) the four rivers. (f) Cumulative distribution function of the fraction of k_{sn} components.

Figure 7. Angles of hillslopes along the trunk stream in each river catchment. The top bar represents channel substrate.

Figure 8. (a) Cumulative frequency of b-axis for particles of sedimentary and volcanic rock. (b) Effect of changing sediment source on the proportion of volcanic particles at the channel bed. The color indicates the ratio of the 84th percentile grain size for the volcanic and sedimentary rock particles measured in each Wolman count. Gray circles are data in Mosawa.

Figure 9. (a–e) Variation of channel width in each river and (f) whole study area. The exponent b in equation 3 is estimated for each river. Local wideness values k_w were calculated using the b value shown in each panel. Circles in (b–f) are colored by channel substrate.

Figure 10. (a) A geologic map around Mosawa and its tributary after 1:50,000 maps (Tsushima & Uemura, 1959; Uemura et al., 1959). Stream data along the solid white lines are used in (c). (b) Proportion of volcanic rock in the upstream catchment. (c) Chi plots for Mosawa and the tributary. Color represents the type of channel substrate. Values of chi and elevation are adjusted so the most downstream point shown in (a) is plotted at the origin.

Table

Table. 1. Channel and sediment characteristics in Tanosawa. The numbers except for D_{84} are median values of the studied section.

	k_{sn} ($m^{0.92}$)	$k_{sn}^{D_s}$ ($m^{0.92}$)	$k_{sn}^{Q_S}$ ($m^{0.92}$)	R (m)	D_{84} (cm)	F_e (%)
Tn1	39.2	12.2	21.3	0.7	19	10
Tn2	20.3	8.1	12.1	0.6	14	20